

## Controlled Pre-Corrosion Attack and Ultrasonic Fatigue Endurance of Titanium Alloy Ti-6Al-4V

### Abstract

Ultrasonic fatigue tests were carried out on titanium alloy Ti-6Al-4V on the base material and the pre-corroded specimen to assess the pre-corrosion effect on the fatigue life of this alloy. The pre-corrosion was obtained by immersion of specimens in an acid solution: hydrochloric acid with 1.4 of pH during 8 and 16 minutes. All ultrasonic fatigue tests were performed following a predetermined sequence to attain the nominal applied load.

Infrared images were taken at the neck section of specimens during ultrasonic fatigue testing, revealing that temperature is higher for the specimens with pre-corrosion and it increases with the time of pre-corrosion. It was observed that pits generated by pre-corrosion were associated with stress concentration, temperature increase and fatigue endurance decrease. Fracture surfaces were analyzed to determine the crack initiation and propagation and the stress intensity factor range threshold  $\Delta K_{TH}$  was obtained for both: the pre-corroded and non pre-corroded specimens.

### Keywords

Ultrasonic fatigue; titanium alloy; corrosion pitting; infrared images; crack initiation and propagation.

Ishvari F. Zuñiga Tello <sup>a</sup>

Gonzalo M. Domínguez Almaraz <sup>a,\*</sup>

Manuel Guzmán Tapia <sup>a</sup>

Jorge L. Avila Ambríz <sup>a</sup>

<sup>a</sup> Facultad de Ingeniería Mecánica, Universidad Michoacana de San Nicolás de Hidalgo (UMSNH), Santiago Tapia No. 403, Col. Centro, Morelia, Michoacán, 58000, México. isfernanda@hotmail.com, dalmaraz@umich.mx, manolo\_verrckt@yahoo.com.mx, joavam@hotmail.com

\* (Corresponding author)

<http://dx.doi.org/10.1590/1679-78253113>

Received 25.05.2016

In revised form 21.11.2016

Accepted 04.01.2017

Available online 09.01.2017

## 1 INTRODUCTION

The alloy Ti-6Al-4V is the most popular titanium alloy for industrial applications. The wide spectrum of uses includes the aerospace industry (Venkateswarlu et al. 2013; Inagaki et al. 2014), marine applications (Gurrappa 2003; Sorokin et al., 1982), biomedical uses (Elias et al. 2008; Assis and Costa 2007), and others (Henry et al. 1995). Frequently, this titanium alloy is subjected to mechanical loading and corrosion (Baragetti 2014; Zavanelli et al. 2000), which lead to a detrimental effect on

fatigue endurance. In order to assess the pre-corrosion effect on the ultrasonic fatigue endurance on this titanium alloy, the testing specimens were immersed in a solution of hydrochloric acid with  $\text{pH} = 1.4$ , for 8 and 16 minutes. All specimens were dried with air after the immersion in the acid solution to avoid additional corrosion attack.

Corrosion pitting is commonly present after corrosion attack on specimens used for fatigue tests (Dominguez-Almaraz et al. 2012; Nový et al. 2013). Recently, some authors have reported a systematic study to evaluate the influence of diverse surface treatment methods on corrosion resistance of the Ti-6Al-4V alloy, after anodic oxidation (Szewczenko et al. 2010). Concerning fatigue endurance results on this titanium alloy, the stress concentration factor  $K_t$  and the notch effects have been investigated under different neutral and corrosion environments for  $2 \times 10^5$  cycles and 10 Hz of frequency (Baragetti 2014). Also, ultrasonic fatigue tests have been reported for this titanium alloy under fully reversed loading conditions at room temperature and atmospheric environment (Morrissey and Golden 2005); others authors have studied the fatigue life and the failure mechanisms of Ti-6Al-4V alloy using ultrasonic technology and 3D laser scanning vibrometry, to obtain non-contact strain measurements during cyclic loading (Heins et al. 2013). Ultrasonic fatigue tests for bimodal and basketweave microstructures have shown that no conventional fatigue limit is observed for the fatigue life range:  $10^5 - 10^9$  cycles; furthermore, beyond one million of cycles of fatigue life the fatigue endurance of bimodal titanium Ti-6Al-4V is higher in regard the basketweave microstructure (Zuo et al. 2008). Nevertheless, no investigations have been developed to assess the corrosion effect on this titanium alloy under ultrasonic fatigue testing.

In this work, pre-corrosion on the ultrasonic fatigue specimens was imposed and special attention was devoted to the geometry and proximity of pre-corrosion pitting, which were revealed strongly associated with the stress concentration, temperature increase and decrease of fatigue endurance. This behavior has been observed for a large number of metallic alloys (Dolley and Dolley 2000; Akid et al. 2006; Zupanc and Grum 2010). Furthermore, most of the stress concentration models for pitting corrosion are related to the geometrical dimensions of one single pit: the depth and width of the pit (Jia et al. 2015; Turnbull et al. 2010). In this work is proposed a model for the stress concentration factors of two or four pits at the neck section of the hourglass shape testing specimen, under uniaxial ultrasonic load.

## 2. EXPERIMENTAL TESTING

### 2.1 Material

Ultrasonic fatigue tests were carried out on the titanium alloy Ti-6Al-4V, which has a microstructure containing primary alpha phase (60%), and lamellar beta combined with secondary alpha phases (40%). The chemical composition (% in weight) and the principal mechanical properties are listed in Table 1 and Table 2, respectively.

The dimensions of the hourglass shape specimen for ultrasonic fatigue were obtained by numerical simulation to fit the resonance condition, which is required for this fatigue testing method. In Figure 1 are shown the obtained dimensions (in mm), for the ultrasonic fatigue testing specimen.

| CHEMICAL COMPOSITION (% IN WEIGHT) |           |      |      |      |       |      |         |
|------------------------------------|-----------|------|------|------|-------|------|---------|
| Al                                 | V         | Fe   | C    | N    | H     | O    | Ti      |
| 5.5 -6.75                          | 3.5 - 4.5 | 0.08 | 0.08 | 0.05 | 0.015 | 0.20 | Balance |
|                                    |           | Max. | Max. | Max. | Max.  | Max. |         |

Table 1: Chemical composition (% in weight) of titanium alloy Ti-6Al-4V.

| PRINCIPAL MECHANICAL PROPERTIES |                                 |                       |                     |                     |                  |                            |
|---------------------------------|---------------------------------|-----------------------|---------------------|---------------------|------------------|----------------------------|
| E<br>[GPa]                      | Density<br>[Kg/m <sup>3</sup> ] | Hardness<br>[Brinell] | $\sigma_y$<br>[MPa] | $\sigma_u$<br>[MPa] | Poisson<br>ratio | Elongation<br>at break [%] |
| 116                             | 4440                            | 95                    | 931                 | 970                 | 0.33             | 10                         |

Table 2: Principal mechanical properties of titanium alloy Ti-6Al-4V.

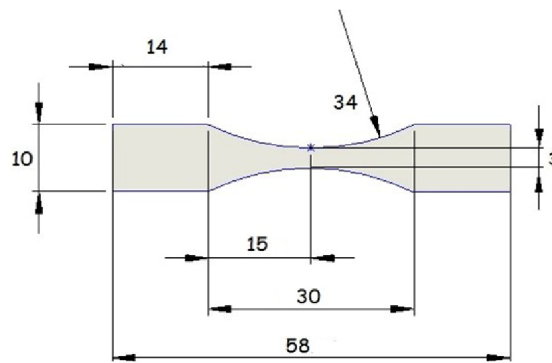


Figure 1: Dimensions (mm), for the ultrasonic fatigue specimen of Ti-6Al-4V.

## 2.2 Ultrasonic Fatigue Testing System

During the ultrasonic fatigue tests, a stationary elastic wave is developed along the testing specimen that induces high stress at the neck section and high displacements at the two ends. The stress and displacement along the testing specimen have been obtained by numerical simulation, as shown in Figure 2. All numerical analysis was carried out on a tridimensional specimen using the Ansys 15.0 software, the tridimensional element SOLID185, automatic meshing and some of the mechanical properties of Table 2 and the dimensions of Figure 1.

A linear relationship was determined between the displacement at the ends of specimen and the high stress induced at the neck section: 1  $\mu\text{m}$  of displacement at the ends generates 12 MPa of stress at the neck section, approximately. Thus, the highest Von Mises stress close to 600 MPa is obtained on the neck section of specimen when the displacement at the ends is of  $\pm 50 \mu\text{m}$ , as shown in Figure 2.

In addition, modal numerical analysis was carried to determine the natural frequency of vibration in longitudinal direction of testing specimen. The Figure 3a presents the result of this modal analysis: 20054 Hz of natural frequency for this titanium alloy using some of the mechanical properties of Table 2 and the dimensions of Figure 1. In Figure 3b is shown the testing specimen attached to the ultrasonic fatigue machine.

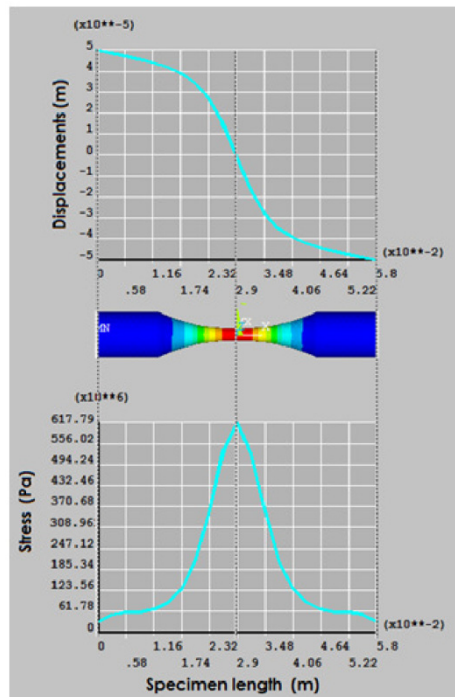


**Figure 2:** Displacement and stress along the titanium alloy Ti-6Al-4V under resonance, obtained by numerical simulation.

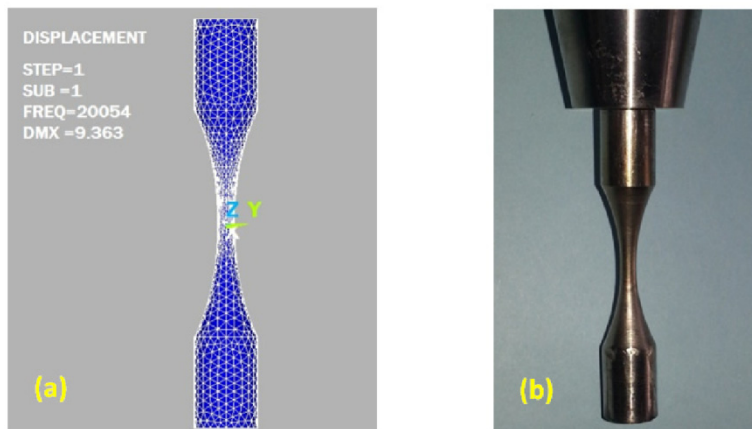


**Figure 3:** a) Natural longitudinal frequency of vibration of Ti-6Al-4V obtained by modal analysis, b) Ultrasonic fatigue testing specimen attached to the testing machine.

All ultrasonic fatigue tests were carried out with a patented machine developed in our laboratory (patent number: 323948, Mexican Institute of Industrial Property, 2014), which is totally controlled by a developed LabVIEW program, allowing the test initiation, the record of the number of cycles in real time and the automatic stop when the specimen fails (Dominguez-Almaraz 2015). Calibration of

testing specimen at the free end was implemented by an inductive proximity sensor which has resolution of  $\pm 2 \mu\text{m}$ , working at 1.5 KHz. All tests were carried out at room temperature (close to  $25^\circ \text{C}$ ), with environmental humidity between 35 and 45% and full reversed load ratio  $R = -1$ .

The sequence for the ultrasonic fatigue tests has been as follow: stabilization of the system for 30 seconds with an applied load of 149 MPa (corresponding to the lower voltage of ultrasonic generator: 10 volts); afterwards, increasing 14.9 MPa each second to attain the nominal applied load. This titanium alloy presents sensibility to the increasing load rate during starting test. The described sequence for the test starting was implemented to fix the conditions of ultrasonic fatigue testing.

### 2.3 Pre-Corrosion Attack

The pre-corrosion attack was imposed to a number of specimens by immersion in hydrochloric acid with 1.4 of pH during 8 and 16 minutes, Figure 4a. All specimens were dried with dry air immediately after immersion to stop the subsequent corrosion. Micrographs for specimens without pre-corrosion and specimens with 8 and 16 minutes of pre-corrosion are shown on Figures 4b, 4c and 4d, respectively.

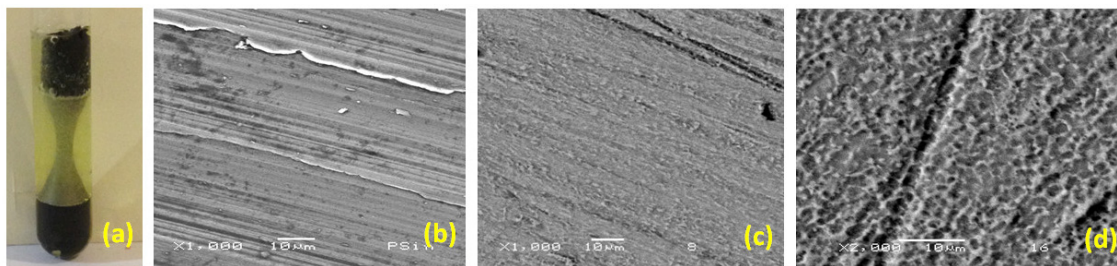


**Figure 4:** a) Pre-corrosion process, b) specimen without pre-corrosion, c) 8 minutes of pre-corrosion, d) 16 minutes of pre-corrosion.

The corrosion rate ( $CR$ , mm/year) is used to estimate the corrosion effect on industrial metallic alloys (Jones 1995; Deng et al. 2012), and is expressed as:

$$CR = \frac{87.6 \Delta wt}{\rho \cdot A \cdot t} \quad (1)$$

Where:

$CR$  is the corrosion rate,

$\Delta wt$  is the weight loss, measured in milligrams,

$\rho$  is the density of titanium alloy in  $\text{g}/\text{cm}^3$ ,

$A$  is the area of corrosion in  $\text{cm}^2$ , and

$t$  is the time of exposure in hours.

The weight losses in milligrams for the two types of pre-corroded specimens were: 8 milligrams for specimens immersed 8 minutes, and 12 milligrams for specimens immersed 16 minutes of pre-

corrosion. The pre-corrosion surface of this specimen has been  $5.34 \text{ cm}^2$ , and:  $\rho = 4.44 \text{ g/cm}^3$ ,  $t = 8$  and  $16$  minutes; thus, the obtained values for CR have been:  $\text{CR} = 221.7 \text{ mm/year}$  for  $8$  minutes of immersion, and  $\text{CR} = 166.3 \text{ mm/year}$  for  $16$  minutes. Corrosion rates comprised between  $40$  and  $230 \text{ mm/year}$  are commonly present in this titanium alloy at room temperature for different uses, such as: chemical, marine and other industrial applications (Gurrappa 2003).

#### 2.4 Measures of Temperature During Ultrasonic Fatigue Testing on Pre-Corroded Specimens and Non-Pre-Corroded Specimens

Important energy dissipation takes place under ultrasonic fatigue testing because of the very high frequency of vibration, which is related to the damping phenomenon. One direct consequence is the temperature increase caused by the high frequency vibration at the neck section of specimen. Temperature at this zone was registered by an infrared camera for two stress levels and for the three types of specimens: non-pre-corroded and pre-corroded with  $8$  and  $16$  minutes of immersion in hydrochloric acid, Figure 5. The last figure shows some images for the two applied loads:  $298$  and  $447 \text{ MPa}$ ; whereas Figure 6 presents the temperature evolution for the three types of specimens in regard the applied load: the results show that temperature increases with applying load and with time of pre-corrosion. Furthermore, an asymptotic behavior seems to be observed for the three types of testing specimens when the applied load reaches the  $450 \text{ MPa}$ .

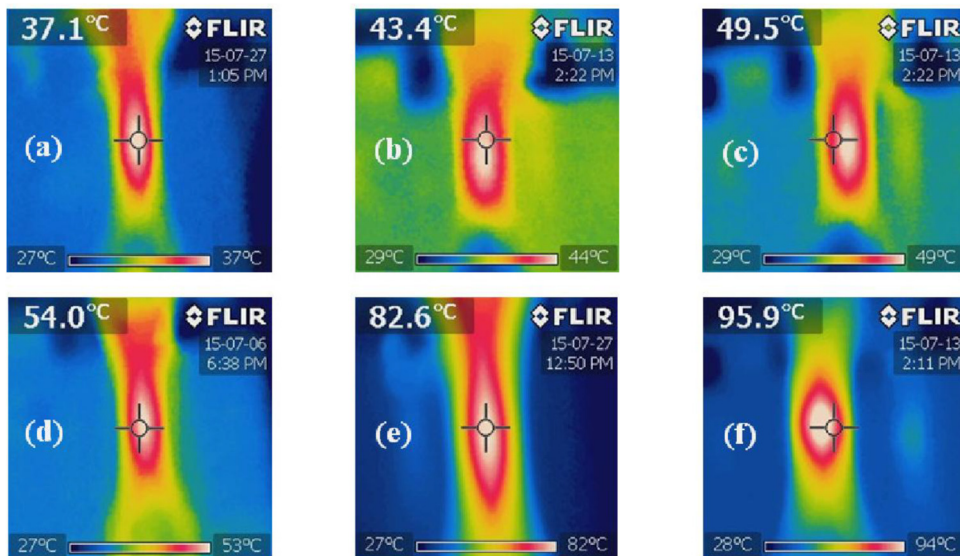


**Figure 5:** Infrared images loading at  $298 \text{ MPa}$  for the specimens: a) Non-pre-corroded, b) Pre-corroded  $8$  minutes, and c) Pre-corroded  $16$  minutes. Thermographic images loaded at  $447 \text{ MPa}$  for the specimens: d) Non pre-corroded, e) Pre-corroded  $8$  minutes and f) Pre-corroded  $16$  minutes.

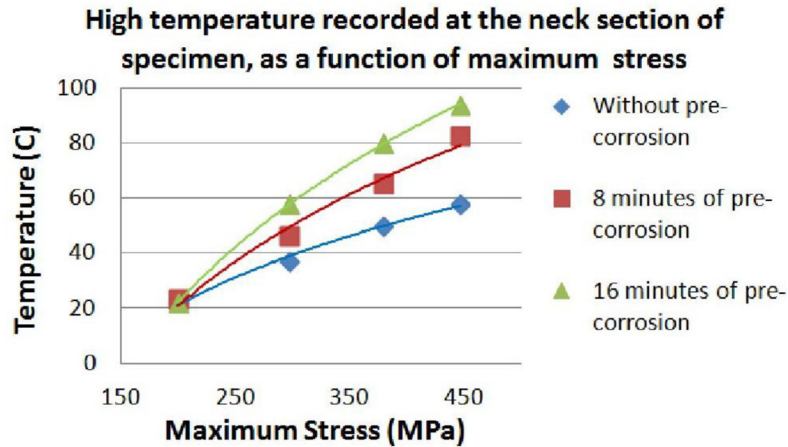


**Figure 6:** Temperature evolution at the neck section of specimen with the applied load and the time of pre-corrosion.

### 3. ULTRASONIC FATIGUE RESULTS ON TITANIUM ALLOY TI-6AL-4V, FOR PRE-CORRODED AND NON CORRODED SPECIMENS

In Figure 7 are plotted the ultrasonic fatigue endurance results for this titanium alloy and for the three testing specimens. The experimental results in this figure show that the ultrasonic fatigue endurance for the pre-corroded specimens decreases compared to non-pre-corroded specimens. For fatigue life of 5 million of cycles (high loading between 560 – 660 MPa), the difference between specimens without pre-corrosion and specimens pre-corroded 16 minutes is close to 100 MPa; whereas for the very high number of cycles (beyond  $10^9$  cycles), the effect of pre-corrosion seems to decrease: at  $2 \times 10^9$  cycles the difference between the two last specimens is only 40 MPa, approximately.

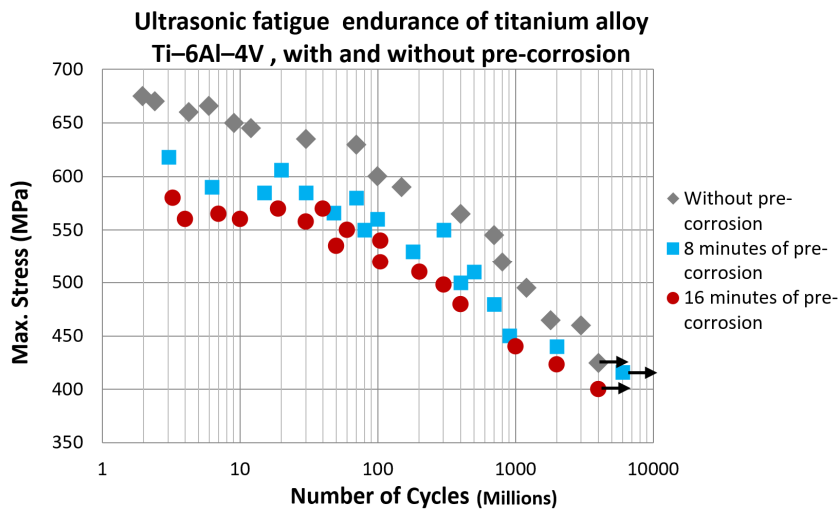


**Figure 7:** Ultrasonic fatigue endurance for titanium alloy Ti-6Al-4V: non-pre-corroded specimens and pre-corroded with hydrochloric acid (pH = 1.4), 8 and 16 minutes.

The origin of this behavior seems to be associated with the pre-corrosion pits, which induces stress concentration at the pre-corroded surface. The stress concentration is related to temperature increase, as observed by the infrared images of Figure 5. In order to assess the general interaction between: pits – stress concentration – temperature increase – and fatigue endurance reduction, a numerical study has been developed and is presented in the next section.

#### 4. DISCUSSION

Pitting associated with stress concentration has been the object of scientific studies, most of them are oriented to investigate the relationship between: the geometrical properties of one single pitting (semi-elliptical or hemispherical), and the stress concentration factors (Cerit et al. 2009; Mu et al. 2010; Zhao et al. 2013). In a recent work has been investigated the stress concentration around perforations produced by corrosion in steel storage tanks (Godoy et al. 2014); which points out that the irregular profiles of pitting can approach an elliptical perforation with two principal parameters: the number  $n$  of “grooves” or “waves” at the inner boundary of the perforation (cosine boundary and star-like boundary), and the deviation “ $d$ ” of the cosine or star-like at the inner boundary. The principal conclusion is that the stress concentration factor tends to highest values when the number of waves “ $n$ ” increases, under uniaxial and shear loading. It is mentioned interaction between waves inside the same perforation when the number of waves  $n$  increases; nevertheless, numerical results are not presented for the case when two or more close perforations are interacting.

Very few studies have been devoted to investigate the proximity of two or more pitting and its effect on the stress concentration factor (Dominguez Almaraz and Pérez Mora 2013; Kolios et al. 2014). In the next section is presented a numerical analysis to investigate the effect of two or more hemispherical pits at the neck section of the hourglass shape specimen of titanium alloy.

The diameter for all simulated hemispherical pitting at the neck section of specimen was  $200\ \mu\text{m}$ , a factor of 10 in regard the physical dimension of the diameter of pitting for the pre-corroded specimens:  $20\ \mu\text{m}$  approximately, Figure 8.

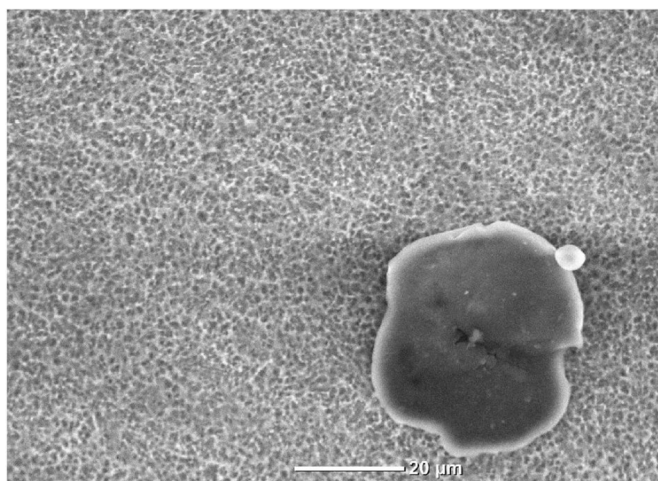


**Figure 8:** SEM image for pitting on the specimen surface: pH = 1.4 and 16 minutes of pre-corrosion.

It was observed that the number of pits increases with the time of pre-corrosion from 8 to 16 minutes, rather than the size of pits. Furthermore, numerical simulations were carried out using different diameters for the pitting: 20, 50 100, 200 and 300  $\mu\text{m}$ ; nevertheless, no important variation was observed on the obtained stress concentration factors under similar condition of loading. The average physical dimension for the pitting diameter corresponds to the grain size of this titanium alloy, that is: 20  $\mu\text{m}$  approximately. Some authors have pointed out that the corrosion attack is primarily developed at the grain boundary (Young and Young 2003; Han et al. 2000).

In Figure 9a is shown the stress distribution for the titanium specimen without hemispherical pits and 30  $\mu\text{m}$  of tension at both ends; whereas in Figure 9b is presented the Von Mises stress distribution with one single pitting under the same tension. Figure 9c shows the Von Mises stress distribution under the same tension and two transverse pits with 50  $\mu\text{m}$  of separation; whereas Figure 9d presents the stress distribution under similar tension at the ends of specimen and two transverse pits, this time with only 20  $\mu\text{m}$  of separation.

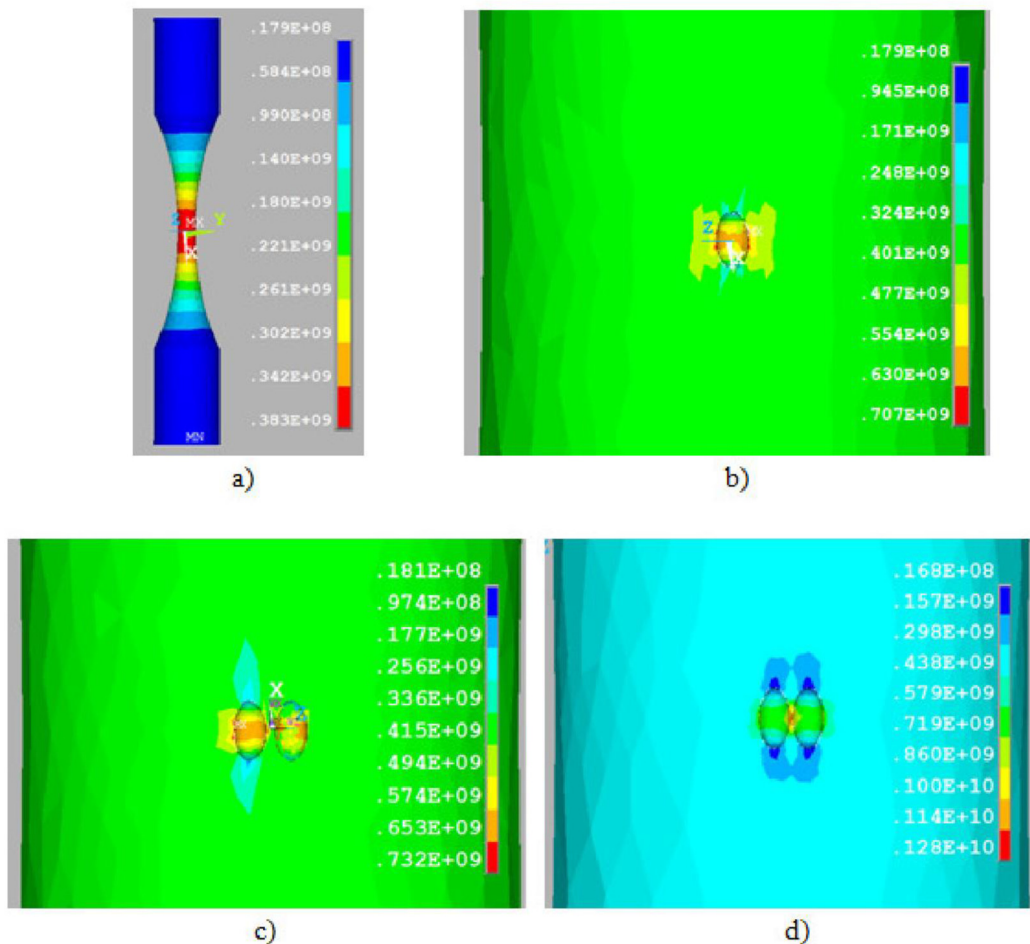


**Figure 9:** Von Mises stress at the neck section of testing specimen with 30  $\mu\text{m}$  of tension at the ends: a) Without pre-corrosion, b) With one single pitting, c) Two transverse pits separated 50  $\mu\text{m}$ , d) Two transverse pits separated 20  $\mu\text{m}$ .

Additional numerical simulations have been obtained concerning four pitting holes: two on transverse direction and two on longitudinal direction in regard the principal axis of testing specimens, separated 50 and 20  $\mu\text{m}$  as shown in Figure 10a and 10b, respectively.

The interaction between two or more hemispherical pits at the surface seems to be an important factor for the stress concentration, in addition of the dimensions and shape of pitting (Dominguez Almaraz and Pérez Mora 2013). Under uniaxial loading, which is the case of this study, transverse pitting and its proximity seems to be the principal factor to increase the stress concentration. The high Von Mises stress for the non-pre-corroded specimen is close to 383 MPa with a tension displacement of 30  $\mu\text{m}$  at the ends of titanium alloy specimen (Figure 9a); this value increases to 707 MPa with a single pitting (Figure 9b), it reaches 732 MPa for two transverse pits separated 50  $\mu\text{m}$  (Figure 9c), and it attains 1280 MPa for two transverse pitting at the neck section of specimen with separation of 20  $\mu\text{m}$  (Figure 9d).

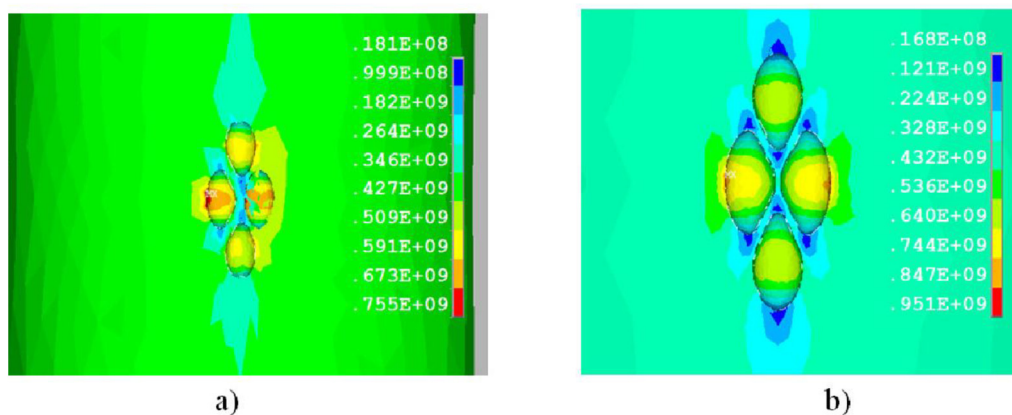


**Figure 10:** Von Mises stress for 4 pits at the neck section of specimen and 30  $\mu\text{m}$  of tension at the ends: a) separation between pits of 50  $\mu\text{m}$ , b) separation between pits of 20  $\mu\text{m}$ .

Additional pits in longitudinal direction seems to induce low modification on the high stress at the neck section of specimen: Figure 10a shows a slight increase of stress for the specimen with 4 pits separated 50  $\mu\text{m}$  compared to Figure 9c; whereas Figure 10b presents a decrease of stress compared to Figure 9d, concerning pits separated 20  $\mu\text{m}$ . In addition, it is observed that the highest stress is located at the bottom of the hemispherical pitting (Figure 9c), and it moves to the front sides of the two pitting when the distance of separation is reduced (Figure 9d). This behavior is modified when longitudinal pits are added, as depicted in Figure 10a and 10b, where highest stresses change to the opposite sides of the two transverse pits.

Thus, the stress concentration increases with the reduction of separation of two transverse pits at the neck section of specimen, undergoing uniaxial tension. Under this loading condition, the addition of longitudinal pits induces low variation or even reduction on the stress, as it is observed on Figure 10b.

It is necessary to remark that all these numerical results have been obtained under uniaxial loading; it is expected an important deviation when applying biaxial or triaxial loading, since interaction between pits in different angles and proximities must be introduced. This will be the subject of a future study.

Concerning the uniaxial loading, a simple model is proposed to assess the stress concentration factor related to the proximity of two transverse pits and two longitudinal pits at the neck section of the specimen. In Figure 11 is shown the stress concentration factor  $K_t$  in the vertical axis and the separation  $d$  between the two hemispherical pits (200  $\mu\text{m}$  of diameter), in transverse or longitudinal direction, plotted on the horizontal axis.

The empirical model for  $K_t$  considering two hemispherical pits in transverse direction without pits in longitudinal direction is as follows:

$$K_t = 1.85 + B \cdot e^{-d/9} \quad (2)$$

Where:

$B$  is a constant = 13.75, and  $d$  is the separation ( $\mu\text{m}$ ) between the two hemispherical pitting holes.

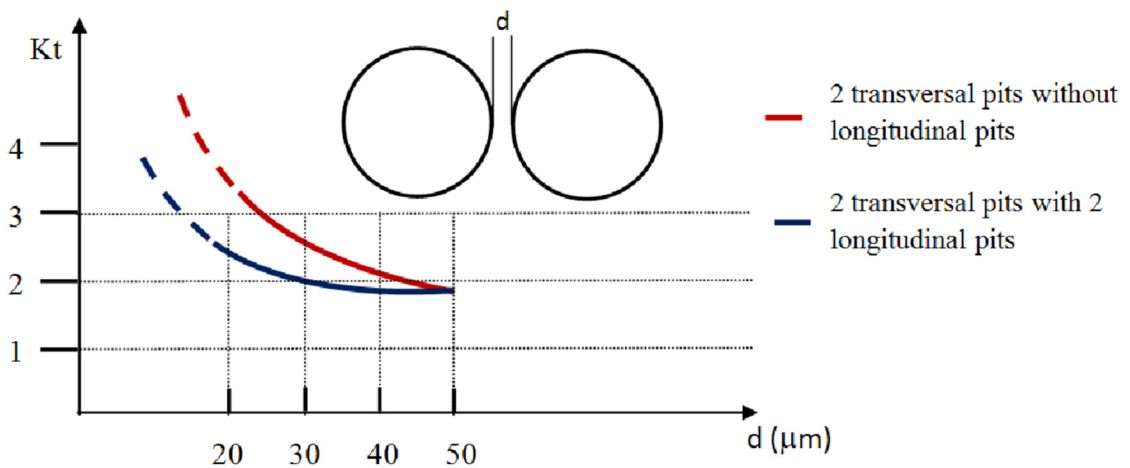


**Figure 11:** Evolution of stress concentration factor  $K_t$  with the separation of two hemispherical pitting in transverse and longitudinal direction at the neck section, with 30  $\mu\text{m}$  of tension at the ends.

The corresponding empirical model for two hemispherical pits in transverse direction with two pits in longitudinal direction (the four pits separated the same distance  $d$ ), is written as:

$$K_t = 1.85 + B \cdot e^{-d/12} \quad (3)$$

This time with:  $B = 3.335$ .

The asymptotic behavior of these models implies that  $K_t$  tends to 1.85 when the separation between the two pits grows up: no interaction of hemispherical pitting at the neck section of specimen in both directions:  $K_t$  corresponds to a single pitting hole, Figure 9b.

In addition, the crack initiation and propagation were analyzed by SEM images as shown in Figure 12. The Figure 12a presents the fracture surface for this titanium alloy tested at 700 MPa of

loading (75% the elastic limit of this alloy), for a specimen attacked with hydrochloric acid (pH=1.4) during 8 minutes. Crack initiation has been reported at the subsurface of specimen under ultrasonic fatigue testing of Ti-6Al-4V titanium alloy: a distance from the surface between 419  $\mu\text{m}$  and 586  $\mu\text{m}$ , no matter the stress amplitude (Heins et al. 2013). Since some of specimens in this work has been subjected to pre-corrosion attack, the crack initiation site for them has been frequently located at the surface of specimen, associated with high stress concentration induced by pitting.

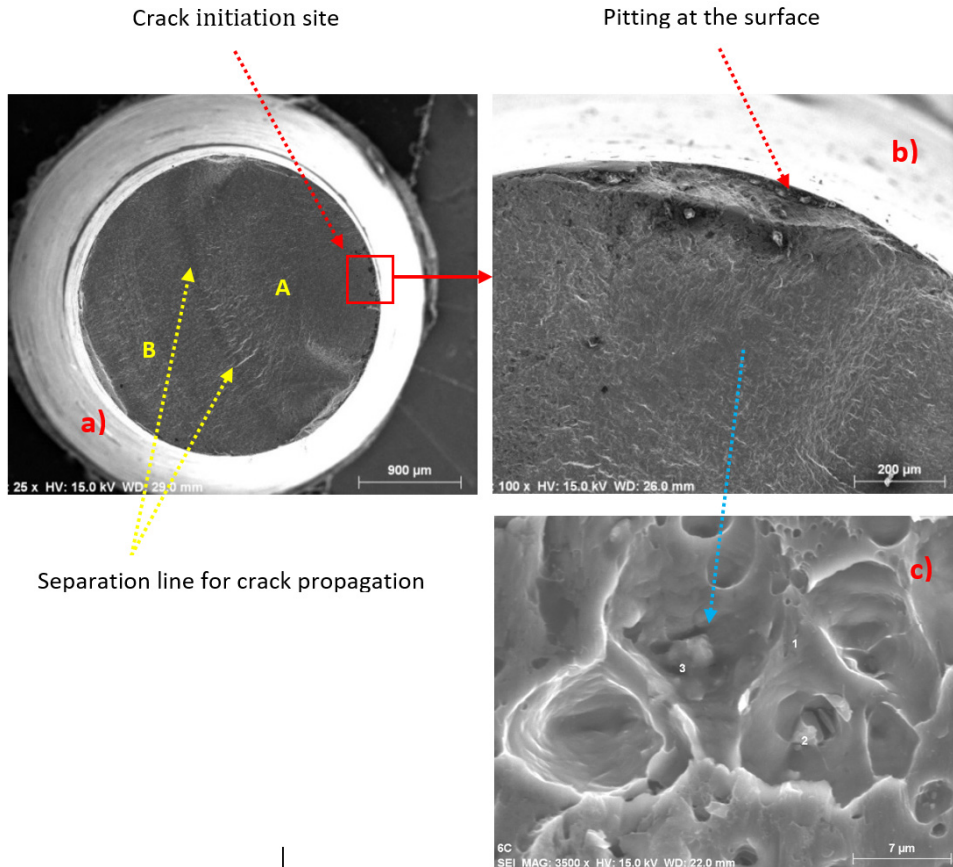


**Figure 12:** a) Fracture surface for the specimen tested at 700 MPa, with immersion in hydrochloric acid (pH=1.4) for 8 minutes, b) site of crack initiation c) Micro-voids coalescence.

The crack initiation site was associated with the high stress concentration at the surface of specimen (presence of pitting generated by pre-corrosion), accompanied with plastic deformation at microscopic scale (micro-voids coalescence), which is observed in Figure 12c (Dominguez-Almaraz et al. 2014; Xue et al. 2002). The nucleation of micro-voids under ultrasonic fatigue leads to micro-cracks, which is the result of shear bands that facilitate the sites of failure inside the regions softened by thermal effect (Xue et al. 2002; Zhang et al. 2011). Furthermore, the line of separation between the ductile-like (zone A) and brittle-like (zone B), of crack propagation is clearly denoted on Figure 12a.

In order to assess the effect of pre-corrosion on the crack initiation threshold of this titanium alloy, large-crack tests ( $a > 3 \text{ mm}$ ), were implemented using the back-face strain compliance technique

(Newman et al. 2011). Tests were carried out on a servo-hydraulic machine, working under close-loop control on K and 50 Hz of frequency. Crack growth tests were obtained at room conditions (23° C and 45% of relative humidity), using the compact test (CT) specimen, following the ASTM E647 standard for the fatigue crack growth rate and the K decreasing test. Three types of compact test specimens were tested: the non-pre-corroded and the specimens with 8 and 16 minutes of pre-corrosion. The dimensions of testing specimen have been selected to correspond to the ASTM E647 standard: B = 6 mm (the thickness of specimen),  $a = 18$  mm (the crack length) and W = 35 mm (the width of the specimen).

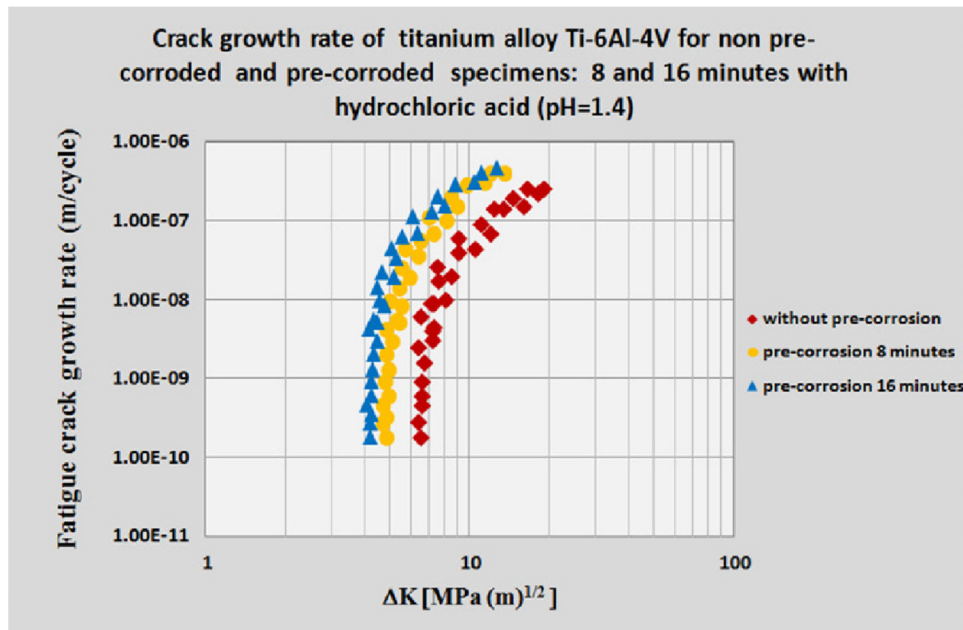


**Figure 13:** Crack growth rates for the titanium alloy Ti-6Al-4V, without pre-corrosion and 8 and 16 minutes of pre-corrosion in hydrochloric acid (pH = 1.4).

In Figure 13 are plotted the crack growth rates for the three tested specimens: the stress intensity factor range threshold  $\Delta K_{TH}$  for the non-pre-corroded specimens under large-crack testing is revealed near to  $6.5 \text{ MPa m}^{1/2}$ , a value close to  $5.9 \text{ MPa m}^{1/2}$  which has been predicted recently by others authors in the case of short fatigue cracks under load ratio  $R = -1$  and  $\sigma_{max} = 650 \text{ MPa}$  (Wang et al. 2014). Concerning the pre-corroded specimens, the stress intensity factor range threshold under large-crack testing has been near to  $4.8 \text{ MPa m}^{1/2}$  for the specimens with 8 minutes of pre-corrosion, and  $4.2 \text{ MPa m}^{1/2}$  for the specimens with 16 minutes of pre-corrosion.

The crack growth tests were carried out considering the so called “large-cracks”, which implies lower growth rates compared to the “small cracks” ( $< 500 \mu\text{m}$ ), under the same applied driving force (Ritchie et al. 1999). Small cracks can propagate below the stress intensity factor range threshold corresponding to large cracks; nevertheless, some small cracks become large cracks with time. The

results obtained herein are devoted to investigate the effect of pre-corrosion on the large-crack growth rates of the Ti-6Al-4V alloy.

## 5 CONCLUSIONS

The following conclusions can be drawn from the present work:

- Ultrasonic fatigue tests have been obtained on non-pre-corroded titanium alloy Ti-6Al-4V, and on specimens with 8 and 16 minutes of pre-corrosion in hydrochloric acid ( $\text{pH} = 1.4$ ).
- The pre-corrosion on this titanium alloy has induced the corrosion rates: 221.7 mm/year and 166.3 mm/year, which are commonly present on this titanium alloy at room temperature for applications in industries, such as: chemical, marine and others.
- The infrared images reveal that stress concentration and temperature increase at the neck section of pre-corroded specimens compared to non-pre-corroded specimens, under similar loading.
- Pre-corrosion pitting is at the origin of the relationship: increase of stress concentration – increase on temperature – decrease on ultrasonic fatigue endurance.
- The ultrasonic fatigue endurance decreases on pre-corroded specimens compared to the non-pre-corroded specimens of this titanium alloy: near to 100 MPa the difference between specimens without pre-corrosion and specimens pre-corroded 16 minutes at 5 million of cycles of fatigue life; this difference is close to 40 MPa when fatigue life attains the  $2 \times 10^9$  cycles.
- An empirical model is proposed to estimate the stress concentration factor  $K_t$ , by the proximity of two hemispherical pitting at the neck section of specimen in transverse and longitudinal direction, in regard the principal axis of specimen.
- Numerical results show that the proximity of two transverse hemispherical pitting holes on the neck section of specimen is critical for the increase of the stress concentration factor  $K_t$ .
- Fracture surfaces show two zones for crack propagation: the ductile-like crack propagation (zone A), characterized by microscopic plastic deformation and containing the crack initiation site, and the brittle-like (zone B), crack propagation where plastic deformation is inexistent.
- Crack growth rates for the three tested specimens were obtained under large-crack testing: the stress intensity factor range threshold  $\Delta K_{TH}$  for the non-pre-corroded specimens has been near to  $6.5 \text{ MPa m}^{1/2}$ , whereas the values for this property have been  $4.8 \text{ MPa m}^{1/2}$  and  $4.2 \text{ MPa m}^{1/2}$  for specimens with 8 and 16 minutes of pre-corrosion, respectively.

## Acknowledgements

The authors express their gratitude to the University of Michoacán in Mexico for the facilities received in the development of this work. A special mention of gratitude to CONACYT (The National Council for Science and Technology, Mexico), for the financial support destined to this study by the program grant: CB- 241117-2014.

## References

Akid R, Dmytrakh IM, Gonzalez-Sanchez J (2006) Fatigue damage accumulation: the role of corrosion on the early stages of crack development. *Corr Eng Sci and Tech* 41(4): 328-335.

- Assis SL, Costa I (2007) Electrochemical evaluation of Ti-13Nb 13Zr, Ti-6Al-4V and Ti-6Al-7Nb alloys for biomedical application by long-term immersion tests. *Mat and Corr* 58(5): 329-333.
- Baragetti S (2014) Notch corrosion fatigue behavior of Ti-6Al-4V. *Materials* 7: 4349-4366.
- Cerit M, Genel K, Eksi S (2009) Numerical investigation on stress concentration of corrosion pit. *Eng Fail Analysis* 16: 2467-2472.
- Deng Q, Shi HW, Ding NN, Chen BQ, He XP, Liu G, Tang Y, Long YT, Chen GR (2012) Novel triazolylbis-amino acid derivatives readily synthesized via click chemistry as potential corrosion inhibitors for mild steel in HCl. *Corros Sci* 57: 220-227.
- Dolley L, Dolley W (2000) The effect of pitting corrosion on fatigue life. *Fat & Fract of Eng Mat & Struct* 23(7): 555-560.
- Dominguez-Almaraz GM (2015) Effect of roughness and residual compression stresses on the ultrasonic fatigue endurance of aluminum alloy AISI 6061-T6. *Mat Perf and Charact* 4(1): 45-60.
- Dominguez-Almaraz GM, Ávila-Ambriz JL, Peyraut F, Cadenas-Calderón E (2012) Effect of controlled corrosion attack with HCl acid on the fatigue endurance of aluminum alloy AISI 6063-T5, under rotating bending fatigue tests. *MRS Procee* 1485: 53-58.
- Dominguez-Almaraz GM, Dueñas Aburto A, Correa Gómez E (2014) Ultrasonic fatigue endurance of aluminum alloy 6061-T6, on pre-corroded and non-corroded specimens. *Metall and Mat Trans A* 45: 280-286.
- Dominguez-Almaraz GM, Pérez Mora R (2013) Ultrasonic fatigue testing on mooring chains steel: effect of corrosion pitting holes and the stress concentration factors. *Int J of Dam Mech* 22: 860-877.
- Elias CN, Lima JHC, Valiev R, Meyers MA (2008) Biomedical applications of titanium and its alloys. *JOM* 60(3): 46-49.
- Godoy LA, Boccardo AD, Rodríguez FJ, Dardati PM (2014) Stress concentration around perforations produced by corrosion in steel storage tanks. *Lat Amer J of Sol and Struct* 11: 1830-1845.
- Gurrappa I (2003) Characterization of titanium alloy Ti-6Al-4V for chemical, marine and industrial applications. *Mat Charat* 51(2-3): 131-39.
- Han Z, Zhao H, Chen XF, Lin HC (2000) Corrosion behavior of Ti-6Al-4V alloy welded by scanning electron beam. *Mat Sci and Eng A* 277(1-2): 38-45.
- Heins S, Balle F, Wagner G, Eifler D (2013) Analysis of fatigue properties and failure mechanisms of Ti6Al4V in the very high cycle fatigue regime using ultrasonic technology and 3D laser scanning vibrometry. *Ultras* 53: 1433-1440.
- Henry SD, Dragolich KS, DiMatteo ND, & ASM International (1995) *Fatigue data book: Light structural alloys*. Materials Park, OH: ASM International: 264-268.
- Inagaki I, Shirai Y, Takechi T, Ariyasu N (2014) Application and features of titanium for the aerospace industry. *Nip Steel & Sumitomo Metal Tech Report No. 106*, July 2014: 22-27.
- Jia J, Zhang Ch, Kodikaraa J, Yang S-Q (2015) Prediction of stress concentration factor of corrosion pits on buried pipes by least squares support vector machine. *Eng Fail Anal* 15: 131-138.
- Jones DA (1995) *Principles and Prevention of Corrosion*, 2nd ed., Prentice-Hall, Upper Saddle River, NJ, 572 pp.
- Kolios A, Srikanth S, Salonitis K (2014) Numerical simulation of material strength deterioration due to pitting corrosion. *Procedia CIRP* 13: 230-236.
- Morrissey R, Golden P (2005) Ultrasonic fatigue testing of Ti-6Al-4V. *J. of ASTM International* 2(5): 1-10.
- Mu ZT, Chen DH, Zhu ZT, Ye B (2010) The stress concentration factor of different corrosion pits shape. *Adv Mat Research* 152-153: 1115-1119.
- Newman JC Jr, Yamada Y, James MA (2011) Back-face strain compliance relation for compact specimens for wide range in crack lengths. *Eng Fract Mech* 78: 2707-2711.

- Nový F, Zatkalíková V, Bokuvka O, Miková K (2013) Gigacycle fatigue endurance of marine grade stainless steels with corrosion pits. *Transport Eng* 41(2): 99-103.
- Ritchie RO, Davidson DL, Boyce BL, Campbell JP, Roder O (1999) High cycle fatigue of Ti-6Al-4V. *Fat & Fract of Eng Mat & Struct.* 22: 621-631.
- Sorkin G, Lane Jr. IR, Cavallaro JL (1982) Ti-6Al-4V for marine uses. *Titanium and Titanium alloys:* 2139-2147.
- Szewczenko J, Walke W, Nowinska K, Marciniak J (2010) Corrosion resistance of Ti-6Al-4V alloy after diverse surface treatments. *Mat Sci & Eng Techn* 41(5): 360-371.
- Turnbull A, Wright L, Crocker L (2010) New insight into the pit-to-crack transition from finite element analysis of the stress and strain distribution around a corrosion pit. *Corr Sci* 52(4): 1492-1498.
- Venkateswarlu V, Tripathy D, Rajagopal K, Tharian KT, Venkitakrishnan PV (2013) Failure analysis and optimization of thermo-mechanical process parameters of titanium alloy (Ti-6Al-4V) fasteners for aerospace applications. *C. Stud in Eng Fail Analysis* 1: 49-60.
- Wang K, Wang F, Cui W, Hayat T, Ahmad B (2014) Prediction of short fatigue crack growth of Ti-6Al-4V. *Fat and Fract of Eng Mat and Struct* 37(10): 1075-1086.
- Xue Q, Meyers MA, Nesterenko VF (2002) Self-organization of shear bands in titanium and Ti-6Al-4V alloy. *Acta Mat* 50: 575-596.
- Young B-S, Young NE (2003) The Effect of heat treatment on the corrosion-resistance for Ti-6Al-4V Alloy. *J. of the Korean Soc of Mar Eng* 27(3): 453-459.
- Zavanelli RA, Pessanha Henriques GE, Ferreira I, de Almeida Rollo JMD (2000) Corrosion-fatigue life of commercially pure titanium and Ti-6Al-4V alloys in different storage environments. *The J of Prosth Dent* 84(3): 274-279.
- Zhang J, Tan Ch-wen, Ren Y, Yu X-dong, Ma H-lei, Wang F-chi, Cai H-nian (2011) Adiabatic shear fracture in Ti-6Al-4V alloy. *Trans. Nonferrous Met. Soc. China* 21: 2396-2401.
- Zhao W, Huang YF, Ye XB, Hu BR, Liu JZ, Chen LJ (2013) Correlation between the geometric parameters of corrosion pit and stress concentration factor. *App. Mechanics and Mat* 327: 156-160.
- Zuo JH, Wang ZG, Han EH. (2008) Effect of microstructure on ultra-high cycle fatigue behavior of Ti-6Al-4V. *Mat Sci and Eng A* 473: 147-52.
- Zupanc U, Grum J (2010) Effect of pitting corrosion on fatigue performance of shot-peened aluminium alloy 7075-T651. *J of Mat Process Techn* 210(19): 1197-1202.